

RESEARCH ARTICLE | APRIL 26 2021

Interlayer configurations of self-assembled folded graphene

Special Collection: [Twisted 2D Electronic and Photonic Materials and Devices](#)

L. Bockhorn  ; J. C. Rode; L. Gnörich; P. Zuo; B. Brechtken; R. J. Haug 

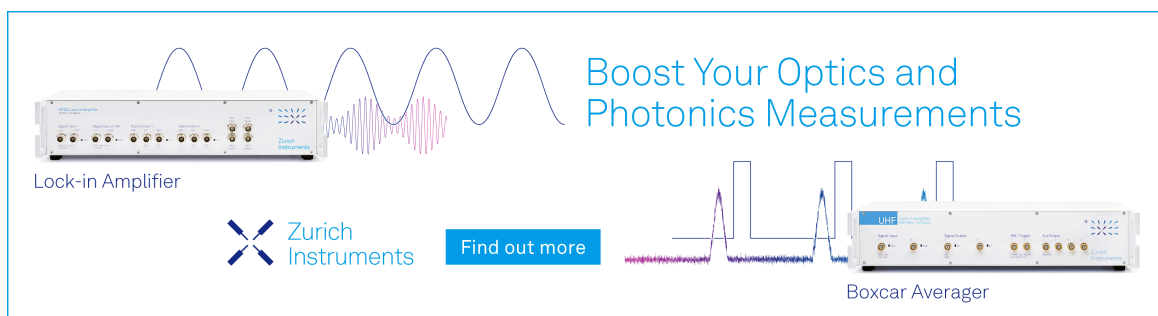


Appl. Phys. Lett. 118, 173101 (2021)

<https://doi.org/10.1063/5.0047602>




CrossMark



Boost Your Optics and Photonics Measurements

Lock-in Amplifier

 Zurich Instruments

[Find out more](#)

Boxcar Averager

Interlayer configurations of self-assembled folded graphene

Cite as: Appl. Phys. Lett. **118**, 173101 (2021); doi: [10.1063/5.0047602](https://doi.org/10.1063/5.0047602)

Submitted: 15 February 2021 · Accepted: 12 April 2021 ·

Published Online: 26 April 2021



View Online



Export Citation



CrossMark

L. Bockhorn,^{a)} J. C. Rode, L. Gnörich, P. Zuo, B. Brechtken, and R. J. Haug

AFFILIATIONS

Institut für Festkörperphysik, Leibniz Universität Hannover, 30167 Hannover, Germany

Note: This paper is part of the APL Special Collection on Twisted 2D Electronic and Photonic Materials and Devices.

^{a)} Author to whom correspondence should be addressed: bockhorn@nano.uni-hannover.de

ABSTRACT

The relative orientation between atomic lattices in twisted bilayer graphene opens up a whole new field of rich physics. So, the study of self-assembled twisted bilayer graphene gives deep insight into its underlying growth process. Cuts in monolayer graphene via the atomic force microscopy technique are used to start self-assembly and to generate a folding process. The final configurations for this self-assembly process are investigated. Here, the focus is on structures that arise from one cut. During the self-assembly, these structures not only move forward but also rotate. As it turns out, the final positions for all studied structures can be assigned to commensurate interlayer configurations.

© 2021 Author(s). All article content, except where otherwise noted, is licensed under a Creative Commons Attribution (CC BY) license (<http://creativecommons.org/licenses/by/4.0/>). <https://doi.org/10.1063/5.0047602>

The stacking and folding of 2D materials to 3D structures enable the tailoring of optical, mechanical, electronic, and magnetic properties. After the first initial experiments on monolayer graphene,^{1,2} different techniques were established to control the 2D-to-3D transformation for graphene. Recently, an advanced microfabrication technique based on the principles of origami^{3–5} and kirigami^{6–8} was introduced. This technique generated astonishing structures with unique properties by precise folding and cutting. The precise control and knowledge of the rotational mismatch between two graphene lattices are essential for the understanding of its electronic properties.^{9–15}

The superposition of two graphene lattices gives rise to a moiré pattern reflecting the honeycomb structure on a larger scale. However, the moiré pattern becomes strictly periodic only at discrete commensurate angles.¹⁶ Commensurate twist angles ϕ_c can be expressed via rotation of two equal-length combinations $\mathbf{p} = m \cdot \mathbf{a}_1 + n \cdot \mathbf{a}_2$ and $\mathbf{q} = m \cdot \mathbf{a}_1 + n \cdot \mathbf{a}_2$ by

$$\cos(\phi_c) = \frac{|\mathbf{p}| \cdot |\mathbf{q}|}{\mathbf{p} \cdot \mathbf{q}} = \frac{1/2 \cdot m^2 + 2mn + 1/2 \cdot n^2}{m^2 + mn + n^2}, \quad (1)$$

where \mathbf{a}_1 and \mathbf{a}_2 are graphene lattice vectors and the integers m and n describe the rotation. The wavelength of a commensurate interlayer configuration can be written as

$$\lambda_c = a_G \cdot \sqrt{m^2 + mn + n^2} = a_G \frac{|r|}{2 \sin(\phi_c/2)}, \quad (2)$$

with a_G being the graphene lattice constant and $r = m - n$ for simplicity. This expression still contains non-primitive structures. To get rid of these structures, only coprime pairs of n and m are allowed. Additionally, there is a commensurate structure of $\sqrt{3}$ -times smaller wavelength with respect to Eq. (2) for every configuration with $r \bmod 3 = 0$ so that the primitive commensurate structures are separated into $r \bmod 3 \neq 0$ (odd) and $r \bmod 3 = 0$ (even). These two sets differ in their sublattice exchange symmetry.¹⁶ A large number of commensurate interlayer configurations are found across the whole angular range.

Here, we focus on the atomic force microscopy (AFM) technique to initiate the self-driven folding process of graphene monolayers.^{17–21} The self-assembled folding process offers a valuable clue about the involved energies. The energetically favorable interlayer configuration of bilayer graphene is Bernal stacking, which represents the prevalent vertical ordering in the unit cell of natural graphite.^{22–25} For twisted bilayer graphene (TBG), it is assumed that the van der Waals interaction energy will drive the system to the most energetically favorable commensurate state.^{26,27} During the folding process, two types of TBG areas are achieved. TBG areas arising from two cuts are nicely explained by an energy minimization model that includes the bilayer adhesion energy density.²¹ In this work, we concentrate on the geometrical analysis of self-assembled folded monolayers with only one cut.

Our graphene samples were prepared by mechanical exfoliation of natural graphite and placed onto a silicon dioxide (SiO₂) substrate.

Suitable graphene monolayers were selected via optical detection.²⁸ Afterward, a diagonal cut was applied through monolayer graphene with a diamond coated probe at a high contact force. This cut initiates the self-assembly, which is monitored using the AFM. The geometry of the final structures is analyzed using AFM and an optical microscope.

A number of methods are known to determine the rotational mismatch between two graphene lattices. We extracted the twist angle from the sample geometry observable in optical images. Therefore, the twist angle ϕ is described by twice the angle φ between the edge of the folded structure and the original sample edge as $\phi = 2 \cdot \varphi$.^{12,14,21} This relation is illustrated in Fig. 1. Here, the left inset shows schematics of such a self-assembled structure. The folded edge (gray dashed line) is viewed as an acting mirror axis between bottom and top layers. Thus, the obtained twist angles are projected into a range of 0 and 30. For statistics over a large number of samples, this method provides a good compromise between experimental effort and information. If two independent, non-connected lattices are investigated by this method, an error of up to 30 in 50% of cases is possible due to the fact that arm-chair and zigzag edges cannot be distinguished. However, in folded structures, the top and bottom layers share the same lattice, which eliminates this need of distinction. Depending on the quality of straight, undisrupted edges in a sample, our accuracy lies in the range of 3. In few cases, higher accuracies around 0.5 were achieved via moiré pattern resolution using the AFM.^{12,14,21}

For this work, the rotational mismatch of 15 TBG areas with one cut was determined mainly from the sample geometry and their results are depicted in Fig. 1. To put our findings into context, we also analyzed TBG structures arising from two cuts and from mechanically stimulated flip-over processes of a whole area of a flake, with no cuts. Flip-overs stabilize typically at a low rotational mismatch, while two-rip structures are preferentially found at twist angles between 20 and 30.^{14,16,21,29} It is assumed that two-rip structures grow in-plane by sliding forward continuously fed by a rolling motion at the folded edge taking advantage of the adhesion energy between the two layers.

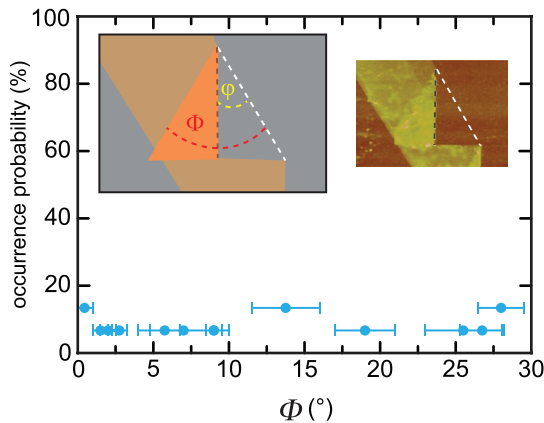


FIG. 1. The occurrence probability of self-assembled monolayer graphene as a function of rotational mismatch. The increment of twist angle ϕ is 0.25. The insets show a scheme of a one-rip structure (left) and the corresponding AFM topography (right). Also shown is the determination of the rotational mismatch between two graphene layers. The twist angle ϕ is twice the angle φ between folded (gray dashed line) and sample edges (white dashed line).

Thereby, the growth process prefers low frictions between top and bottom graphene layers to compensate energy loss. Low friction is associated with incommensurate interlayer configurations.^{21,30–32}

In contrast to the other folding processes,¹⁴ a clear twist angle dependence is not observed for the one-rip structures as seen in Fig. 1. They are evenly and seemingly randomly distributed. In this work, we focus on the evolution of such one-rip structures. We demonstrate our findings on different snapshots of self-assembled folded monolayers. On the basis of several AFM images like the ones shown in Fig. 2, we conclude the underlying folding process.

The one-rip structure formation shown in Fig. 2 was recorded with a diamond coated probe at moderately elevated force in the AFM. The folding process was initiated during contact-mode scanning in the intermediate repulsive range of tip-sample interaction. Figure 2(a) shows a downscan of the final static TBG area. The corresponding upscan (18.75 nm s⁻¹) in the trace direction (19.2 μ ms⁻¹) of this triangular fold in evolution is seen in Fig. 2(b). The contour of the final TBG area to evolve is marked by transparent white lines in Fig. 2(b). Above the upper dashed line (113 s), the recorded folding geometry is identical to the final one as depicted in Fig. 2(a). Below the lower

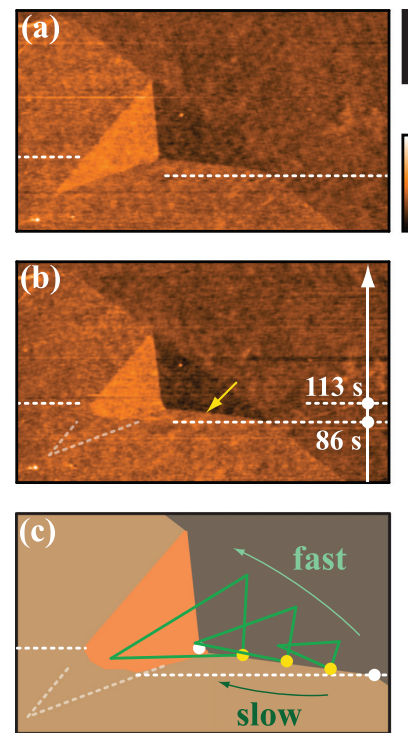


FIG. 2. AFM topography of one self-assembled folded graphene monolayer with a rotational mismatch of around 2, the color scale spans 4.5 nm, and the scale bar indicates 2 μ m; (a) downscan of the final folded configuration and (b) upscan in the trace direction. The upscan shows a snapshot of the TBG area evolution, and its final contour is indicated in transparent white. Above the upper dashed white line (113 s), the main topographic features compared to the final configuration are already developed. In between dashed lines, geometry of the torn vacancy to the right appears identical, while the folded area to the left is in evolution. (c) Schematic of intermediate folded configurations in the time frame between white dots. The folding direction rotates counterclockwise.

dashed white line (86 s), no sign of a fold is observed. These two observations indicate formation of the folded TBG area in a time frame of roughly 30 s, as elapsing between the dashed white lines. The topographic features resolved in the respective local and temporal window furthermore allow for reconstruction of the likely scenario of growth. Based on our observations in Fig. 2(b) in between the dashed lines, we suggest a counterclockwise rotation in the direction of the folded edge as depicted in Fig. 2(c). In this schema, we demonstrate that the self-assembly leads not only to a folded TBG area marked by the green triangles but also at the same time to a rotation. The initiation of the folding process by a small cut is marked by the right white point. The folded TBG area would remain above and beyond a given linescan at its lower right corner (yellow dots). In this scenario, the absence of elevated topography below the torn edge is accounted for. For this proposed rotation, different growth velocities are assumed along the native sample edge to the top and the torn edge to the bottom.

One advantage of our measurement setup is deep insight into the underlying growth process due to the fact that there are less hard boundary conditions, except for scan speed, cut angle, and contact force. So, the self-assembled growth process is dominated by interlayer stacking. To understand under which conditions this self-assembly process comes to a stop, we analyzed the twist angles of the final structures. Not only is the completely different folding mechanism of one-rip structures in contrast to two-rip structures^{20,21} astonishing but also the observed twist angles. Contrary to the clear assignment of twist angles to the incommensurate interlayer configuration for two-rip structures, the situation for one-rip structures is not that obvious. However, one can speculate that the one-rip structures are locked to commensurate configurations. To get deeper insight into the final interlayer configuration, we determine the wavelength of a commensurate interlayer configuration concerning Eq. (2) for each twist angle. In the other cases, the index pair (n, r) was selected so that the discrepancy between calculated and measured twist angles is small [Eq. (2)]. Figure 3(a) shows commensurate structures in a parameter space window of indices $(n, r) \leq (100, 100)$ depending on the twist angle ϕ and the corresponding commensurate wavelength λ_c ; yellow dots are odd, and blue dots are even interlayer configurations. The determined twist angles of the examined one-rip structures are depicted as red dots, including their corresponding errors in the parameter space window. Based on our assumptions, it looks like that all the examined one-rip structures may in fact be assigned to a commensurate angle of low wavelength. So, we assume that the self-assembly process comes to a stop if a commensurate configuration is reached, i.e., the commensurate locking of the two lattices stops the folding process. At small twist angles, commensurate configurations grow increasingly dense in twist angle, which leads to an inevitable match at the smallest possible wavelength defined by moiré wavelength Eq. (2). In Fig. 3(b), small-angle structures ($\Phi < 5$) are omitted from the assignment to reduce the range of wavelengths for a better resolution. This magnification of the lowest wavelength illustrates the assignment of twist angles to commensurate configurations. Only the lowest generations of commensuration are required to find matches for angles of rotational mismatch. This observation leads to the assumption of growth under rotation and termination of sliding

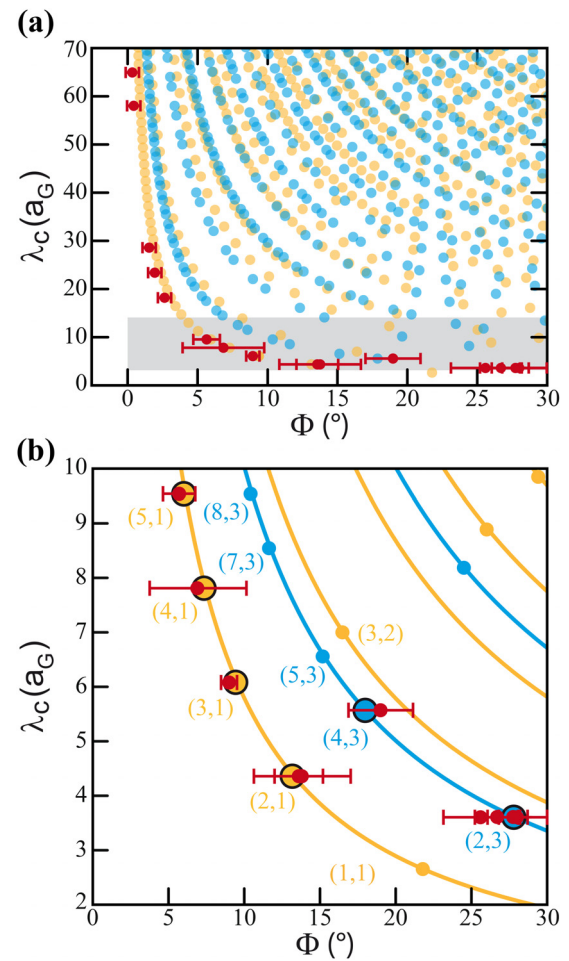


FIG. 3. Assignment of twist angles in one-rip structures to commensurate configurations. (a) Yellow (odd configurations) and blue (even configurations) dots indicate wavelength λ_c vs rotational mismatch Φ for the entirety of commensurate structures [identified via index pairs $(n, r) \leq (100, 100)$] within the depicted parameter window. Rotational mismatches found in our samples are depicted as red dots. Here, the corresponding commensurate wavelength λ_c was calculated using Eq. (2), while the index pair (n, r) was selected, with n and r being smallest. At low rotational mismatches, the availability of matches is inevitable due to the increasing density of commensurate structures. (b) Therefore, the five lowest twist angles are omitted to clarify the assignment to commensurate interlayer configurations in a magnification.

expansion in commensurate lock, which is consistent with the prediction of Peymanirad *et al.*²⁷ for thermal activated rotation of large graphene flakes on graphene. However, until now, only the AB stacking was found after thermal activation as a commensurate state.²⁶ Also, for graphene on top of hexagonal boron nitride, a transition from the incommensurate to commensurate configuration is observed but only for small rotational mismatches ($\Phi < 1$).³³

Another example of the dynamic evolution of one-rip structures is seen in Fig. 4. Here, a downscan of a rectangular graphene flake is shown after the one-rip structure reached its final configuration. The

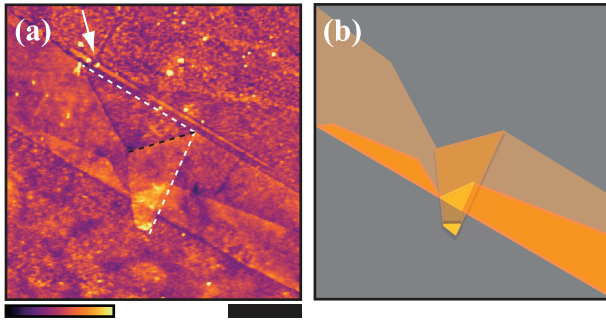


FIG. 4. (a) AFM topography of a one-rip structure, the color scale spans 4 nm, and the scale bar indicates 2 μm . A diagonal cut at a high contact force was applied perpendicular to the upper edge, indicated by the white arrow. The former and the final flake position are marked by dashed lines. The evolved structure not only slides over an additionally TBG area but also over the substrate. Thereby, the upper layer of the TBG area is torn and a second one-rip structure arises. In panel (b) the final configuration of the one-rip structure is illustrated schematically.

lower part of the rectangular graphene flake consists of a TBG area obtained during the exfoliation process. To initiate the self-assembled growth process, a diagonal cut was applied perpendicular at a high contact force through the graphene monolayer. The remaining of the cut is marked by a white arrow in the AFM topography. The position of the starting point for the growth process was selected so that the resulting folded monolayer must slide over the already existing TBG area to prove the high process energy. During the self-assembly process, the primary one-rip structure slides forward over the TBG area and starts to rip its upper graphene layer. A second one-rip structure is observed beneath the primary one. The process energy must be so high that not only a second one-rip structure is initiated but also a slide forward across the substrate. Additionally, the dynamical evolution of the primary one-rip structure shows a clockwise rotation of the fold. Based on the downscan during the evolution process, the one-rip structure rotates clockwise. In its final configuration, the tip of the primary one-rip structure flipped over. This folding process is presumably triggered by scanning the final graphene flake with the AFM probe or it is caused by the rough substrate surface.

Self-assembled folded graphene is assumed to be more rigid in the lateral plane than a flake without a folded edge. Therefore, a higher homogeneity over the whole flake area is achieved, which is necessary for the fabrication of electronic devices based on TBG. Here, our focus is the self-assembled folding process with less hard boundary conditions, and so we get deep insight into the favorable final interlayer configurations. One-rip structures rotate during the evolution process. These rotations and the possible assignment of twist angles to commensurate configurations suggest a conservation of energy by finding efficient configurations. Consequently, the folded edge rotates during the progressive folding process to stabilize finally in a commensurate configuration. This efficient folding process also enables a forward sliding motion of the upper graphene layer on difficult territories, e.g., on substrates.

The realization of the super-moiré pattern is, in principle, possible by the AFM technique. Such structures are accidentally achieved during the folding process or by applying a second cut. To make use of

such more complicated structures, further studies are needed in the future.

Normally, there is a small parameter uncertainty of our boundary conditions, e.g., the cut angle that varies over a few degrees. Consequently, there might be a connection between the cut angle variations and the final rotational mismatch. It would be interesting to analyze this dependence in more detail.

This project was funded by the Deutsche Forschungsgemeinschaft (DFG, German Research Foundation) under Germany's Excellence Strategy-EXC-2123 QuantumFrontiers-390837967 and within the Priority Program SPP 2244 "2DMP."

DATA AVAILABILITY

The data that support the findings of this study are available from the corresponding author upon reasonable request.

REFERENCES

- ¹K. S. Novoselov, A. K. Geim, S. V. Morozov, D. Jiang, Y. Zhang, S. V. Dubonos, I. V. Grigorieva, and A. A. Firsov, *Science* **306**, 666 (2004).
- ²A. K. Geim and K. S. Novoselov, *Nat. Mater.* **6**, 183 (2007).
- ³T. W. Ebbesen and H. Hiura, *Adv. Mater.* **7**, 582 (1995).
- ⁴S. Cranford, D. Sen, and M. J. Buehler, *Appl. Phys. Lett.* **95**, 123121 (2009).
- ⁵H. Chen, X.-L. Zhang, Y.-Y. Zhang, D. Wang, D.-L. Bao, Y. Que, W. Xiao, S. Du, M. Ouyang, S. T. Pantelides, and H.-J. Gao, *Science* **365**, 1036 (2019).
- ⁶T. Castle, Y. Cho, X. Gong, E. Jung, D. M. Sussman, S. Yang, and R. D. Kamien, *Phys. Rev. Lett.* **113**, 245502 (2014).
- ⁷M. Bles, A. Barnard, P. Rose, S. P. Roberts, K. L. McGill, P. Y. Huang, A. R. Ruyack, J. W. Kevek, B. Kobrin, D. A. Muller, and P. L. McEuen, *Nature* **524**, 204 (2015).
- ⁸S. Chen, J. Chen, X. Zhang, Z.-Y. Li, and J. Li, *Light Sci. Appl.* **9**, 75 (2020).
- ⁹J. M. B. Lopes dos Santos, N. M. R. Peres, and A. H. Castro Neto, *Phys. Rev. Lett.* **99**, 256802 (2007).
- ¹⁰J. D. Sanchez-Yamagishi, T. Taychatanapat, K. Watanabe, T. Taniguchi, A. Yacoby, and P. Jarillo-Herrero, *Phys. Rev. Lett.* **108**, 076601 (2012).
- ¹¹Y. Kim, H. Yun, S.-G. Nam, M. Son, D. S. Lee, D. C. Kim, S. Seo, H. Cheul Choi, H.-J. Lee, S. W. Lee, and J. S. Kim, *Phys. Rev. Lett.* **110**, 096602 (2013).
- ¹²H. Schmidt, J. C. Rode, D. Smirnov, and R. J. Haug, *Nat Commun.* **5**, 5742 (2014).
- ¹³J. C. Rode, D. Smirnov, H. Schmidt, and R. J. Haug, *2D Mater.* **3**, 035005 (2016).
- ¹⁴J. C. Rode, D. Smirnov, C. Belke, H. Schmidt, and R. J. Haug, *Ann. Phys.* **529**, 1700025 (2017).
- ¹⁵Y. Cao, V. Fatemi, S. Fang, K. Watanabe, T. Taniguchi, E. Kaxiras, and P. Jarillo-Herrero, *Nature* **556**, 43 (2018).
- ¹⁶E. J. Mele, *Phys. Rev. B* **81**, 161405 (2010).
- ¹⁷E. Hamm, P. Reis, M. LeBlanc, B. Roman, and E. Cerda, *Nat. Mater.* **7**, 386 (2008).
- ¹⁸D. Sen, K. S. Novoselov, P. M. Reis, and M. J. Buehler, *Small* **6**, 1108 (2010).
- ¹⁹O. Kruglova, F. Brau, D. Villers, and P. Damman, *Phys. Rev. Lett.* **107**, 164303 (2011).
- ²⁰J. Annett and G. L. W. Cross, *Nature* **535**, 271 (2016).
- ²¹J. C. Rode, D. Zhai, C. Belke, S. J. Hong, H. Schmidt, N. Sandler, and R. J. Haug, *2D Mater.* **6**, 015021 (2018).
- ²²J. M. Campanera, G. Savini, I. Suarez-Martinez, and M. I. Heggge, *Phys. Rev. B* **75**, 235449 (2007).
- ²³Y. Shibuta and J. A. Elliott, *Chem. Phys. Lett.* **512**, 146 (2011).
- ²⁴J. Berashevich and T. Chakraborty, *Phys. Rev. B* **84**, 033403 (2011).
- ²⁵K. Uchida, S. Furuya, J.-I. Iwata, and A. Oshiyama, *Phys. Rev. B* **90**, 155451 (2014).
- ²⁶M. Zhu, D. Ghazaryan, S.-K. Son, C. R. Woods, A. Misra, L. He, T. Taniguchi, K. Watanabe, K. S. Novoselov, and Y. Cao, *2D Mater.* **4**, 011013 (2016).
- ²⁷F. Peymanirad, S. K. Singh, H. Ghorbanfekr-Kalashami, K. S. Novoselov, F. M. Peeters, and M. Neek-Amal, *2D Mater.* **4**, 025015 (2017).

- ²⁸P. Blake and E. W. Hill, *Appl. Phys. Lett.* **91**, 063124 (2007).
- ²⁹J. M. B. Lopes dos Santos, N. M. R. Peres, and A. H. Castro Neto, *Phys. Rev. B* **86**, 155449 (2012).
- ³⁰M. Hirano and K. Shinjo, *Phys. Rev. B* **41**, 11837 (1990).
- ³¹M. Dienwiebel, G. S. Verhoeven, N. Pradeep, J. W. M. Frenken, J. A. Heimberg, and H. W. Zandbergen, *Phys. Rev. Lett.* **92**, 126101 (2004).
- ³²Z. Liu, J. Yang, F. Grey, J. Z. Liu, Y. Liu, Y. Wang, Y. Yang, Y. Cheng, and Q. Zheng, *Phys. Rev. Lett.* **108**, 205503 (2012).
- ³³C. R. Woods, L. Britnell, A. Eckmann, R. S. Ma, J. C. Lu, H. M. Guo, X. Lin, G. L. Yu, Y. Cao, R. V. Gorbachev, A. V. Kretinin, J. Park, L. A. Ponomarenko, M. I. Katsnelson, Y. N. Gornostyrev, K. Watanabe, T. Taniguchi, C. Casiraghi, H.-J. Gao, A. K. Geim, and K. S. Novoselov, *Nat. Phys.* **10**, 451 (2014).